Pseudo-Jahn-Teller origin of the low barrier hydrogen bond in $N_2H_7^+$

P. García-Fernández,[1,a)] L. García-Canales,[1,2] J. M. García-Lastra,[3] J. Junquera,[1] M. Moreno,[1] and J. A. Aramburu[1]

[1]*Departamento de Ciencias de la Tierra y Física de la Materia Condensada, Universidad de Cantabria, 39005 Santander, Spain*
[2]*Departamento de Química Física y Analítica, Universidad de Oviedo, 33006 Oviedo, Spain*
[3]*Departamento de Física de Materiales, Facultad de Químicas, Universidad del Pais Vasco, 20018 San Sebastián, Spain*

The microscopic origin and quantum effects of the low barrier hydrogen bond (LBHB) in the proton-bound ammonia dimer cation $N_2H_7^+$ were studied by means of *ab initio* and density-functional theory (DFT) methods. These results were analyzed in the framework of vibronic theory and compared to those obtained for the Zundel cation $H_5O_2^+$. All geometry optimizations carried out using wavefunction-based methods [Hartree–Fock, second and fourth order Möller–Plesset theory (MP2 and MP4), and quadratic configuration interaction with singles and doubles excitations (QCISD)] lead to an asymmetrical $H_3N–H^+\cdots NH_3$ conformation (C_{3v} symmetry) with a small energy barrier (1.26 kcal/mol in MP4 and QCISD calculations) between both equivalent minima. The value of this barrier is underestimated in DFT calculations particularly at the local density approximation level where geometry optimization leads to a symmetric $H_3N\cdots H^+\cdots NH_3$ structure (D_{3d} point group). The instability of the symmetric D_{3d} structure is shown to originate from the pseudo-Jahn–Teller mixing of the electronic $^1A_{1g}$ ground state with five low lying excited states of A_{2u} symmetry through the asymmetric α_{2u} vibrational mode. A molecular orbital study of the pseudo-Jahn–Teller coupling has allowed us to discuss the origin of the proton displacement and the LBHB formation in terms of the polarization of the NH_3 molecules and the transfer of electronic charge between the proton and the NH_3 units (rebonding). The parallel study of the $H_5O_2^+$ cation, which presents a symmetric single-well structure, allows us to analyze why these similar molecules behave differently with respect to proton transfer. From the vibronic analysis, a unified view of the Rudle–Pimentel three-center four-electron and charge transfer models of LBHBs is given. Finally, the large difference in the N–N distance in the D_{3d} and C_{3v} configurations of $N_2H_7^+$ indicates a large anharmonic coupling between α_{2u}-α_{1g} modes along the proton-transfer dynamics. This issue was explored by solving numerically the vibrational Schrödinger equation corresponding to the bidimensional $E[Q(\alpha_{2u}),Q(\alpha_{1g})]$ energy surface calculated at the MP4/6-311++G** level of theory. © *2008 American Institute of Physics.* [DOI: 10.1063/1.2980053]

I. INTRODUCTION

Proton transfer is a key process in many important reactions such as acid-base neutralization and enzymatic reactions, the abnormal high proton mobility in aqueous solutions (Grotthuss mechanism), the autoionization in water, rearrangement in photostabilizers, and proton pumping through membrane protein channels.[1] In many cases the proton-transfer reaction can be described as motion through a double-well adiabatic potential energy surface (APES) along the hydrogen-bond (HB) coordinate, which in practical cases has to be corrected taking into account solvent and temperature effects as well as tunneling.[1]

Despite the great quantity of experimental and theoretical works, many details of these processes at a microscopic level remain elusive due to their complexity. In this sense, high level *ab initio* studies on simple model systems presenting a low barrier [when compared to the zero-point energy

(ZPE)] HB (LBHB) can lead to valuable information about the microscopic origin and quantum effects of the proton-transfer reactions and the nature of the HB. One such system is the protonated ammonia dimer $N_2H_7^+$ present in nature in different phases. It is found in the gas phase in the atmosphere of the Earth and other planets where it plays a role in the intermediate steps of some atmospheric reactions.[2] It is also present in liquids such as ammonia,[3] and in solids such as ammonium perchlorate, a solid-state proton conductor, in an ammonia-rich environment,[4] N_2H_7I,[5] zeolitic materials,[6] polyxometalates,[7] and inside a largely hydrophobic supramolecular environment.[8] A deeper knowledge of the proton dynamics in the $N_2H_7^+$ unit is also of interest in other closely related problems. For example, there is a controversy on the role played by LBHB interactions in biological reactions. In cases like the His-12-His-119 pair in ribonuclease[9] it has been hypothesized that LBHB formed by N–H⸳⸳N interaction play an important catalytic role. This interpretation has been challenged by Warshel *et al.*,[10] who supported that the key to the catalytic power of certain proteins is due to their

    129, 124313-1

shape that makes unnecessary polarizing the environment and thus avoids an extra free energy penalty.

Since $N_2H_7^+$ is a floppy molecule, it is difficult to establish its geometry. In order to clarify this question, Price *et al.*[11] carried out a detailed analysis of infrared vibrational measurements on the $N_2H_7^+$ molecular cation concluding that the most likely structure is the symmetric $H_3N\cdots H^+\cdots NH_3$ with D_{3d} symmetry, the central proton being placed midway between both N atoms. By contrast, all the *ab initio* calculations performed to calculate the APES have led to a double-well potential, that is, a $H_3N-H^+\cdots NH_3$ asymmetric structure with C_{3v} symmetry.[12–15] In later works, proton transfer between the two NH_3 moieties was found in molecular dynamics calculations at different levels of theory.[4,15,16] In particular, Asada *et al.*[15] took into account the quantum effects on the wave-packet dynamics along the one-dimensional $E(\xi)$ APES, where ξ is the intrinsic reaction coordinate (IRC), computed at the MP2 level. These authors concluded that $N_2H_7^+$ has a symmetric D_{3d} structure, in agreement with the experimental spectra by Price *et al.*,[11] the contradiction with the minimum energy structure found by geometry optimizations being due to the neglect of quantum effects of the proton in earlier calculations. Recently, Asmis *et al.*[17] provided a joined experimental and theoretical study addressing the consequences of this quantum-mechanical symmetrization through the ZPE. Their four-dimensional anharmonic model agrees well with experimental data, thus providing a first assignment for the main absorption bands.

By contrast, in the proton-bound water dimer $H_5O_2^+$ (Zundel ion), which plays important role in the dynamics of aqueous solutions,[18,19] the ground state presents a single-well APES as reported from both experimental measurements.[20] and high level *ab initio* calculations.[21] The single-well APES of this cation (isoelectronic with $N_2H_7^+$) corresponds to a $H_2O\cdots H^+\cdots OH_2$ structure with two strong nonlinear HBs and C_2 symmetry.

The main goal of the present work is to understand why $N_2H_7^+$ presents a LBHB (double-well APES with transfer of the proton between the two NH_3 moieties) while $H_5O_2^+$ is stable in the symmetric C_2 structure (single-well APES). In addition to perform *ab initio* calculations on both systems we have paid particular attention to analyze their results under the framework of the pseudo-Jahn–Teller (PJT) effect.[22,23] This method, whose application has been largely ignored in this field, allows one to rationalize the different behaviors observed for $N_2H_7^+$ and $H_5O_2^+$. Many works on molecular and solid-state systems[22–25] show that the analysis of the excited states coupled to the ground state via appropriate vibrational modes provide valuable knowledge on the causes giving rise to asymmetric (off-center) atomic displacements. Moreover, conclusions on the electrostatic/covalent (or localized/delocalized) nature of strong HBs can be extracted from this analysis.

The vibronic analysis can also give a relevant insight into the proton dynamics in $N_2H_7^+$. Previous studies[18] indicate that proton transfer is not simply related to a single reaction coordinate that takes H^+ from one ligand to the other

but also that the breathing mode that controls the distance between these ligands plays a very important role. Therefore, another goal of this work will be to carry out a detailed study of the mechanisms behind this coupling and to show whether the infrared spectrum[17] can be understood just using these two modes or if the coupling to a larger number of modes is required to adequately account for all the observed bands.

The present article is arranged as follows. In Sec. II the computational details of the *ab initio* and DFT calculations carried out in the present work are described, while results of the calculations are presented and discussed in Sec. III that has been subdivided in five parts. The results of the geometry optimizations performed on $N_2H_7^+$ and $H_5O_2^+$ are discussed in Secs. III A and III B, respectively, including a test on the reliability of DFT methods to describe the low barrier at the double-well APES for the proton transfer in $N_2H_7^+$.[13] A brief introduction to the basic concepts and notation of vibronic coupling theory and PJT effect[22] is provided in Sec. III C. The origin of the barrier of the double-well APES in $N_2H_7^+$ is analyzed in Sec. III D. A PJT view will allow us to correlate the displacement of the proton with the change in the charge distribution and analyze the different polarization and covalent contributions to the HB formation in $N_2H_7^+$. Using the orbital vibronic constants obtained from *ab initio* calculations, we identify the orbitals which are mainly involved in producing the distortion. From this analysis, a unified view of well established models in this field, like the three-center-four-electrons (3c-4e),[26–28] charge transfer (CT) (Refs. 29 and 30) and valence bond (VB) (Refs. 10, 28, and 31) models, will be given. The lack of barrier in the APES of $H_5O_2^+$ is discussed in Sec. III E. Section III F is devoted to examine quantum effects of the proton motion along the barrier in $N_2H_7^+$. Finally, main conclusions are summarized in Sec. IV.

II. COMPUTATIONAL DETAILS

The time-independent Schrödinger equation for $N_2H_7^+$ and $H_5O_2^+$ molecular cations has been solved under the framework of the adiabatic approximation. In a first step, the energy surface of the ground state was explored using several *ab initio* and DFT methods. Moreover, we carried out several calculations to obtain some relevant excited electronic configurations and reveal their PJT vibronic coupling to the ground state. In a second step, the quantum vibrational dynamics corresponding to the ground state APES have been simulated.

The electronic structure calculations of the ground state were performed using the GAUSSIAN-98 suite of programs.[32] Standard all-electron split-valence basis sets of $6\text{-}31+G^*$ and $6\text{-}311++G^{**}$ quality, which include diffuse and polarization functions to make the basis sets more flexible, were used as supplied in GAUSSIAN-98. Some calculations were performed using the Dunning's correlation consistent triple zeta basis set augmented with diffuse function, aug-cc-pVTZ,[33] which lead to similar results as those obtained with $6\text{-}311++G^{**}$. *Ab initio* calculations have been performed at various levels

TABLE I. Structural parameters for stable C_{3v} (normal letter) and transition state D_{3d} (italic letter) structures of $N_2H_7^+$ obtained with different quantum chemistry (HF, MP2, MP4, and QCISD methods) and DFT (LDA, PW91, BLYP, and B3LYP functionals) calculations. R_D, R_A, R, r_D and r_A distances (in Å) and β_D and β_A angles (in deg) are defined in Fig. 2. Values of the energy barrier between C_{3v} and D_{3d} conformations, ΔE, (in kcal/mol) are also given.

Calculation	R_D	R_A	R	r_D	r_A	β_D	β_A	ΔE
HF/6-31+G*	1.053	1.792	2.845	1.010	1.006	110.0	112.7	4.79
	1.297	*1.297*	*2.594*	*1.008*	*1.008*	*111.6*	*111.6*	
HF/6-311++G**	1.056	1.766	2.822	1.009	1.005	110.0	112.6	3.68
	1.295	*1.295*	*2.590*	*1.007*	*1.007*	*111.6*	*111.6*	
MP2/6-31+G*	1.098	1.675	2.773	1.025	1.022	110.3	112.9	1.71
	1.310	*1.310*	*2.620*	*1.024*	*1.024*	*111.7*	*111.7*	
MP2/6-311++G**	1.120	1.575	2.694	1.021	1.019	110.6	113.1	0.71
	1.299	*1.299*	*2.599*	*1.020*	*1.020*	*111.9*	*111.9*	
MP4/6-31+G*	1.083	1.723	2.806	1.025	1.022	110.3	112.9	2.69
	1.307	*1.307*	*2.614*	*1.024*	*1.024*	*111.8*	*111.8*	
MP4/6-311++G**	1.101	1.623	2.723	1.026	1.023	110.2	113.1	1.26
	1.298	*1.298*	*2.596*	*1.019*	*1.019*	*111.9*	*111.9*	
QCISD/6-311++G**	1.101	1.624	2.726	1.022	1.020	110.5	113.2	1.26
	1.299	*1.299*	*2.598*	*1.020*	*1.020*	*112.0*	*112.0*	
LDA/6-311++G**	1.304	1.306	2.610	1.031	1.031	111.4	111.4	0.00
	1.304	*1.304*	*2.608*	*1.029*	*1.029*	*111.5*	*111.5*	
PW91/6-311++G**	1.277	1.350	2.627	1.026	1.026	111.4	111.8	0.00
	1.312	*1.312*	*2.624*	*1.026*	*1.026*	*111.6*	*111.6*	
BLYP/6-311++G**	1.191	1.492	2.683	1.029	1.028	110.0	112.3	0.16
	1.323	*1.323*	*2.645*	*1.028*	*1.028*	*111.6*	*111.6*	
B3LYP/6-311++G**	1.144	1.548	2.692	1.022	1.020	110.6	112.4	0.41
	1.310	*1.310*	*2.619*	*1.026*	*1.026*	*111.6*	*111.6*	

of theory, increasing the electronic correlation level: Hartree–Fock (HF), Møller–Plesset of second (MP2) and fourth (MP4) orders of perturbation, and quadratic configuration interaction with single and double excitations (QCISD). On the other hand, DFT calculations were carried out using four conventional exchange-correlation functionals: Vosko–Vilk–Nusair[34] in the local density approximation (LDA), Perdew–Wang 1991 (PW91) (Ref. 35) and Becke–Lee–Yang-Parr (BLYP) (Refs. 36) in the generalized gradient approximation (GGA), and the hybrid (including part of the exact HF exchange) three-parameter B3LYP.[37]

Calculations of excited electronic configurations have been performed by means of the Amsterdam density functional (ADF) code[38] using the B3LYP functional. At difference with Gaussian, this code allows us to choose specific electronic configurations in a simple way. Basis sets of TZP quality containing three Slater-type basis functions plus a polarization one per atomic orbital, as implemented in the ADF program, were used.

In order to understand the quantum effects associated with the proton transfer, we have calculated the vibrational levels associated with the motion of the system along the α_{2u} and α_{1g} normal modes of the D_{3d} configuration, associated respectively with the motion of the proton and the breathing mode of the NH_3 units. The bidimensional ground state APES in these normal coordinates, $E[Q(\alpha_{2u}), Q(\alpha_{1g})]$, was computed by means of MP4 calculations on a numerical grid. Then, a finite difference method was applied to solve the corresponding vibrational Schrödinger equation

$$\left\{ -\frac{1}{2}\left(\frac{\partial^2}{\partial Q(\alpha_{2u})^2} + \frac{\partial^2}{\partial Q(\alpha_{1g})^2} \right) \right.$$
$$\left. + E[Q(\alpha_{2u}), Q(\alpha_{1g})] \right\} \theta[Q(\alpha_{2u}), Q(\alpha_{1g})]$$
$$= E_{v(\alpha2u)v(\alpha1g)} \theta[Q(\alpha_{2u}), Q(\alpha_{1g})]. \quad (1)$$

The kinetic energy operator has been represented through a $(n \times m) \times (n \times m)$ Fornberg matrix,[39] where $n=65$ and $m=92$ are the number of points of the grid of calculations along $Q(\alpha_{2u})$ and $Q(\alpha_{1g})$ coordinates, respectively. The Hamiltonian matrix given in Eq. (1) was diagonalized to obtain the vibrational level energies $E_{v(\alpha2u)v(\alpha1g)}$ (depending on the quantum numbers of the α_{2u} and α_{1g} modes) and nuclear wavefunctions $\theta[Q(\alpha_{2u}), Q(\alpha_{1g})]$ for the proton motion. These calculations have been performed on a single-CPU PC using a MATLAB program[40] that takes less than a minute to run.

III. RESULTS AND DISCUSSION

A. Geometry optimizations in $N_2H_7^+$

Structural parameters obtained in the geometry optimizations performed on the $N_2H_7^+$ cation are shown in Table I, while the meaning of the symbols can be seen in Fig. 1. With the exception of the DFT-LDA optimization, the rest of methods predict that the global minimum of the APES is a linearly arranged $H_3N-H^+\cdots NH_3$ C_{3v} conformation with the proton placed closer to one of the NH_3 groups and that there is a small barrier between two equivalent minima. The
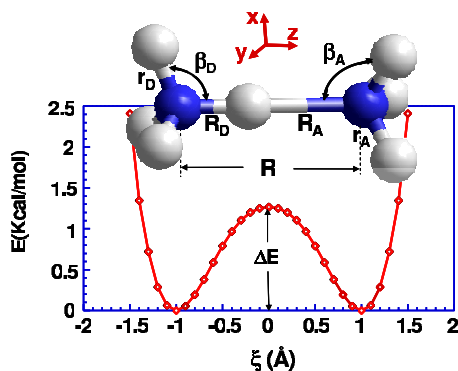
FIG. 1. (Color online) Stable C_{3v} structure of the $N_2H_7^+$ molecular cation and double-well APES along the IRC ξ obtained by means of MP4/6-311++G** calculations.

two NH_3 units are staggered with respect to one another, as shown in Fig. 1. In general, the covalent N–H bond lengths on the proton donor and acceptor NH_3 units, r_D, r_A, and R_D, (Fig. 1) become longer by inclusion of the electron correlation effects so that the bound proton slightly moves to the center of the N_D–N_A bond. The angles β_D and β_A (Fig. 1) do not depend significantly on the computational level in our calculations. The ground state is $^1A_1$ corresponding to a closed-shell electronic configuration. Restricted optimizations in D_{3d} symmetry have also been performed in order to obtain the symmetric $H_3N\cdots H^+\cdots NH_3$ transition state structure in between the two equivalent C_{3v} minima. The ground state for this configuration is $^1A_{1g}$. Results in Table I are in agreement with values obtained in previous *ab initio* calculations on $N_2H_7^+$ at various levels of theory.[12–15]

Structural parameters related to N–H covalent bonds inside ammonia (r_D, r_A, and R_D distances, and β_D and β_A angles) have a small dependence on the quality of the basis set while the HB distance R_A is very strongly dependent on it. In Table I we can observe that R_A decreases when passing from 6-31+G* to 6-311++G** basis set. This effect is more pronounced, the better correlation is taken into account in the calculation. For example, values $R_A=1.723$ and 1.623 Å were obtained for the stable structure at MP4/6-31+G* and MP4/6-311++G** levels of theory, respectively. The dependence of all structural parameters on the quality of the basis sets is much smaller in DFT calculations, as it is well known from previous works.[41] Some test calculations performed using the aug-cc-pVTZ basis lead to similar results that 6-311++G** ones.

Since experimental values of distances and angles are unknown, QCISD results can be considered as the reference parameters. Recent benchmark calculations[42] on a database of barrier heights, which represent a test to calculation methods much more severe than bond energies, have shown that calculations using this method are in excellent agreement with experimental data. Accepting this fact, we can observe that the accuracy of the results (Table I) decreases with the diminution of electronic correlation of the theory, following the series QCISD≈MP4>MP2>HF.

However, structural parameters obtained using DFT methods are different from QCISD ones, and the differences increase following the series B3LYP<BLYP<PW91

<LDA. Moreover, all DFT calculations performed in this work significantly underestimate the barrier energy, especially LDA ($\Delta E=0.00$ kcal/mol, leading to a stable D_{3d} symmetrical structure) and GGA ($\Delta E=0.16$ kcal/mol) functionals. These results are consistent with previous DFT calculations showing that LDA, GGA, and even the popular hybrid functionals (as B3LYP) often lead to failures in the description of numerous properties, especially in the case of low barriers or wells.[42,43] Since the proton-transfer barrier (that determined the transfer rates) of a simple system as $N_2H_7^+$ is poorly determined through DFT based calculations, caution must be taken when simulating the dynamics of condensed phase systems by means of these methods.

The frequencies of all 21 vibrational modes of both the stable and transition state structures have been computed at the MP4/6-311++G** level (see supplemental information[44]). The α_{2u} mode of the D_{3d} structure has an imaginary frequency, $\hbar\omega(\alpha_{2u})=993i$ cm^{-1}. This mode has a stretching character and corresponds to the asymmetric displacement of the proton (the rest of atomic positions remain almost fixed), producing an instability of the symmetric conformation. It is worth noting that the instability driven by the α_{2u} mode is also accompanied by a significant increase ($\sim 5\%$) in the distance R between the two ammonia molecules (Fig. 1). In fact, if the $N_2H_7^+$ molecule is forced to be in the D_{3d} symmetrical configuration, then R is found to be 2.596 Å at the MP4/6-311++G** level. By contrast, R =2.723 Å when the α_{2u} distortion is allowed (Table I). This result indicates that the unstable α_{2u} mode is anharmonically coupled to the breathing mode (associated to the N–N distance, Fig. 1) α_{1g} having a lower frequency, $\hbar\omega(\alpha_{1g})$ =575 cm^{-1}. As discussed in Sec. III F, this fact strongly influences the vibrational dynamics and frequencies.

In Fig. 1 it is also shown the one-dimensional APES computed along the IRC describing the proton transfer from one ammonia molecule to the other. This curve has been calculated at the MP4/6-311++G** level following the steepest descend path associated to the instability of the α_{2u} mode at the D_{3d} configuration. The activation energy ΔE for the proton-transfer process is largely dependent on the computational level as shown in Table I. In the case of *ab initio* methods, ΔE values approximately halve when the quality of the basis sets is increased. For example, ΔE values of 2.69 and 1.26 kcal/mol were obtained at MP4/6-31+G* and MP4/6-311++G** levels of theory, respectively.

At MP4/6-311++G** level of theory the value of the reaction energy of the HB formation process, $NH_4^++NH_3$ $\rightarrow N_2H_7^+$ (C_{3v} conformation), is 26.3 kcal/mol, confirming that a strong HB is formed in $N_2H_7^+$. Although quantum effects on the proton transfer will be analyzed in Sec. III C, their importance can be now advanced. We can have a simple estimation of the ZPE of the α_2 mode as $(1/2)\hbar\omega(\alpha_2)$ =1010 cm^{-1} and scale it by the recommended empirical factor of 0.91.[45] Then, the ZPE, 2.89 kcal/mol, is greater than the barrier $\Delta E=1.26$ kcal/mol indicating that the proton fluctuates freely between both minima.
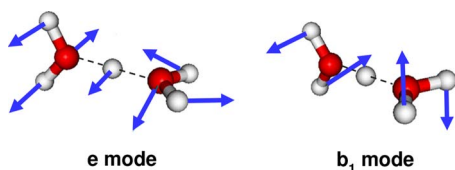
FIG. 2. (Color online) D_{2d} conformation of H$_5$O$_2^+$ that is stable under the b_2 vibrational mode corresponding to the H$^+$ off-center movement. However, it is unstable with respect to b_1- and e-type vibrations that lead to the C_2 and C_s stationary points of the APES, respectively.

B. Geometry optimizations in H$_5$O$_2^+$

Structural calculations have also been carried out for the H$_5$O$_2^+$ cation, isoelectronic to N$_2$H$_7^+$. Only the most relevant results will be presented in the text since they are in agreement with those previously reported in literature.[13,14,21] A summary of our results can be found in the supplemental information. In H$_5$O$_2^+$ the analogous configuration to the D_{3d} one in N$_2$H$_7^+$ has D_{2d} symmetry (Fig. 2). There are two lower energy conformers, with C_s and C_2 symmetries (Fig. 1 in supplemental information), which are the ones usually discussed in literature. At the Hartree–Fock level, the C_s geometry, in which the proton is more closely bonded to one oxygen than to the other, is lowest in energy. However, using higher-level *ab initio* calculations H$_5$O$_2^+$ presents a C_2 minimum geometry H$_2$O$\cdots$H$^+\cdots$OH$_2$ with two strong nonlinear HBs, in agreement with experimental results.[19] This fact contrasts with the results obtained for N$_2$H$_7^+$, where the stable structure corresponds to a H$_3$N–H$^+\cdots$NH$_3$ asymmetric structure. Calculations on H$_5$O$_2^+$ at the MP4/aug-cc-pVTZ level of theory lead to the following values (see complete results in the supplemental information): $\angle$OHO$=173.6°$ and $R_D=R_A=1.198$ Å for the C_2 stable structure (^1A ground state), while $\angle$OHO$=175.6°$, $R_D=1.198$ and $R_A=1.276$ Å for the C_s conformation ($^1A'$ ground state). The energy difference between both structures is only 0.47 kcal/mol, while the D_{2d} configuration lies 1.39 kcal/mol above the C_2 ground configuration. Results corresponding to MP4/6-311++G** calculations are very similar.

C. Vibronic coupling treatment of high symmetry instabilities

Bersuker showed[22] that any instability of a high-symmetry configuration in any polyatomic system is related to the coupling between electronic and nuclear motions. This vibronic coupling is often of Renner–Teller or Jahn–Teller type for degenerate states in linear and nonlinear systems, respectively, and of PJT type for nondegenerate states. In both N$_2$H$_7^+$ and H$_5$O$_2^+$ systems the high-symmetry conformations (D_{3d} and C_2, respectively) are nonlinear with an orbital nondegenerate ground state Γ_0 (A_{1g} and A, respectively). This state Γ_0 (of energy E_0) mixes with excited states Γ_1 (energy E_1) of appropriate symmetry when the system is distorted along the normal mode represented by Q. This PJT effect[22] can easily be formulated using second-order perturbation, theory, where the energy is expanded around the (reference) equilibrium high symmetry configuration ($Q=0$) as

$$E(Q) = E_0 + \tfrac{1}{2}KQ^2 + \cdots . \tag{2}$$

Here, K is the force constant associated to the vibration represented by Q. K can be expressed as the sum of two terms

$$K = K_0 + K_v. \tag{3}$$

If we define W as the sum of the nuclear-electronic and nuclear-nuclear interactions of the potential energy operator, then the primary force constant K_0 is

$$K_0 = \left\langle \Gamma_0 \left| \frac{\partial^2 W}{\partial Q^2} \right| \Gamma_0 \right\rangle, \tag{4}$$

and K_v is the vibronic coupling contribution

$$K_v = 2\sum_I \frac{\left| \left\langle \Gamma_0 \left| \frac{\partial W}{\partial Q} \right| \Gamma_I \right\rangle \right|^2}{E_0 - E_I}, \tag{5}$$

where the sum extends over all excited states I. K_0 is equal to the force constant that a system would have if the electron density was frozen to its value at $Q=0$. According to Bersuker,[22] K_0 is always positive and represents the force opposing the distortion. K_v represents the contribution to the force constant due to the change in the electron density to adapt to the distorted geometry. For the ground state E_0-E_I is always negative, so K_v is negative. Since $K_0>0$, a necessary condition of instability is that the curvature of $E(Q)$ at $Q=0$ is negative, then $K_0<|K_v|$. In our system the ground state, Γ_0, belongs to the totally symmetric representation and the distortion mode has A_{2u} symmetry, so only coupling to A_{2u} states make $\langle\Gamma_0|\partial W/\partial Q|\Gamma_I\rangle\neq0$ and contribute to the instability.

Direct calculation of the vibronic coupling matrix elements involved in PJT models is mathematically difficult and requires explicit knowledge of the excited states, which may be difficult to obtain. The calculation can be greatly simplified assuming that the excited state wavefunction $|\Gamma_I\rangle$ differs from the ground state one $|\Gamma_0\rangle$ by just a one-electron excitation, $\varphi_i \rightarrow \varphi_j$.[43] In this case, we can approximate the force constant in state I by

$$K_I = K_0 + \sum_{i,j} (n_i^{(I)} - n_j^{(I)}) \frac{|\langle\varphi_i|dv/dQ|\varphi_j\rangle|^2}{\Delta_{ij}^{(I)}}$$
$$= K_0 + \sum_{i,j} (n_i^{(I)} - n_j^{(I)})K_v^{ij}, \tag{6}$$

where $n_i^{(I)}$ is the population of orbital φ_i in state I, v is the interaction potential between one electron and the nuclei, $\Delta_{ij}^{(I)}$ is the transition energy when one electron is taken from φ_i and placed in φ_j, and K_v^{ij} is the vibronic contribution to the force constant due to the coupling of orbitals i and j. What this formula tells us is that if one electron is excited from orbital a to b, which is vibronically coupled to the first, we would find that the force constant of the excited state has *increased* by $2K_v^{ab}$. This way, using Eq. (6) and calculating the force constants of the ground and excited electronic configurations, we can find which orbitals are more involved in the distortion by checking when the force constant varies more strongly. Thus, using Eq. (6), we can consider approxi-
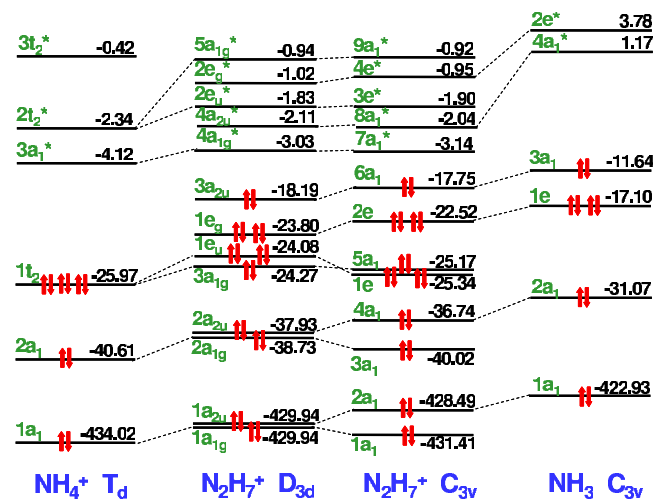
NH$_4^+$ T$_d$

3t$_2$*   -0.42
2t$_2$*   -2.34
3a$_1$*   -4.12
1t$_2$ -25.97
2a$_1$ -40.61
1a$_1$ -434.02

N$_2$H$_7^+$ D$_{3d}$

5a$_{1g}$*   -0.94
2e$_g$*   -1.02
2e$_u$*   -1.83
4a$_{2u}$*   -2.11
4a$_{1g}$*   -3.03
3a$_{2u}$ -18.19
1e$_g$ -23.80
1e$_u$ -24.08
3a$_{1g}$ -24.27
2a$_{2u}$ -37.93
2a$_{1g}$ -38.73
1a$_{2u}$ -429.94
1a$_{1g}$ -429.94

N$_2$H$_7^+$ C$_{3v}$

9a$_1$*   -0.92
4e*   -0.95
3e*   -1.90
8a$_1$*   -2.04
7a$_1$*   -3.14
6a$_1$ -17.75
2e   -22.52
5a$_1$ -25.17
1e   -25.34
4a$_1$ -36.74
3a$_1$ -40.02
2a$_1$ -428.49
1a$_1$ -431.41

NH$_3$ C$_{3v}$

2e*   3.78
4a$_1$*   1.17
3a$_1$ -11.64
1e   -17.10
2a$_1$ -31.07
1a$_1$ -422.93

FIG. 3. (Color online) Diagram (not to scale) depicting the variation in one-electron energy levels going from N$_2$H$_7^+$ in C$_{3v}$ and D$_{3d}$ structures to the dissotiation of NH$_4^+$ (left) and NH$_3$ (right). Energy of every level (in eV units) is also shown. Asteriks mean antibonding orbitals for the bond along the N–H–N axis.

mately the influence of each electron independently on the nuclear framework and its dynamics, providing a more intuitive picture of the electronic processes involved in the distortion compared to the case when full multielectronic states are used. Moreover, an interpretation in terms of orbitals means that the results are transferable to systems with similar orbital schemes, something that is not easily done through full multistate calculations. A more detailed analysis of formula (6) and its consequences is given in Ref. 46.

A qualitative and quantitative orbital analysis of the PJT mechanism of the $D_{3d} \rightarrow C_{3v}$ instability in N$_2$H$_7^+$ will be carried out in the following subsection. Arguments to understand the stability of the symmetric C_2 structure in H$_5$O$_2^+$ will be also given in Sec. III E.

D. Analysis of the $D_{3d} \rightarrow C_{3v}$ instability in N$_2$H$_7^+$

In Fig. 3 we compare the one-electron levels (calculated at the MP4/6-311++G** level) of NH$_4^+$ (T_d symmetry) and NH$_3$ (C_{3v} symmetry) with those of N$_2$H$_7^+$ in the symmetric D_{3d} and asymmetric C_{3v} structures. NH$_4^+$ and NH$_3$ are two isoelectronic closed-shell molecules with rather similar molecular orbital diagrams, but they present two main differences. On one hand, the levels in NH$_4^+$ are shifted $\sim 10-14$ eV toward lower energies when compared to those of NH$_3$. This can be explained taking into account the presence of an extra proton in this molecule that lowers the orbitals by $-e^2/r \sim -10$ eV, assuming a proton-electron distance $r \approx 1$ Å. On the other hand, the t_2 orbital in NH$_4^+$ is split into a_1 and e in NH$_3$ due to the lack of tetrahedral symmetry in the latter.

As the reaction NH$_4^+$ + NH$_3 \rightarrow$ N$_2$H$_7^+$ progresses (Fig. 3), the orbitals coming from NH$_4^+$ and NH$_3$ fragments get closer in energy as the proton is increasingly shared between them. At large distances, occupied orbitals coming from the NH$_3$ fragment experience a strong decrease in energy (about 6 eV for the stable structure) mainly because of the increase in the electrostatic interaction with the ionic charge of the

NH$_4^+$ fragment. Since the NH$_3$ fragment is neutral, this stabilization energy is largely compensated by the repulsion of the proton with the nuclei in this fragment. By contrast, the increase in energy of occupied orbitals coming from the NH$_4^+$ fragment is only about 0.5–1.4 eV, indicating a smaller reorganization of charge in this unit.

Let us analyze the $D_{3d} \rightarrow C_{3v}$ instability of N$_2$H$_7^+$. From a global point of view, the physical effect behind the instability is that the proton passes from being equally bonded to two N atoms to be more covalently bonded to only one of them and forming one HB. Alternatively, this electron redistribution can be understood as the polarization of the electronic cloud of the system favoring the formation of stronger bonds in a C_{3v} NH$_4^+$–NH$_3$ system versus the weaker HBs in the transition state D_{3d} structure H$_3$N$\cdots$H$^+\cdots$NH$_3$ (rebonding effect). This situation is similar to that found in the off-center movement of transition metal impurities in fluorite-type crystals where the transition metal complex passes from cubal to nearly square-planar geometry.[24] In the latter case, it was shown[24] that the microscopic origin of the distortion is a PJT vibronic coupling (through a τ_{1u} mode) of the partially occupied d orbitals of the metal with two kind of orbitals: (a) Fully unoccupied p orbitals of metal that polarize the electronic distribution around the metal favoring the formation of stronger bonds with fewer ligands and (b) rebonding with fully occupied p levels of four ligands placed in a face of the cube.

Let us consider the PJT mechanism of the $D_{3d} \rightarrow C_{3v}$ instability produced by the the α_{2u} mode. According to Eq. (6), there are two types of orbital couplings associated to this vibrational mode: a_{1g}-a_{2u} and e_g-e_u. In particular, the α_{2u} mode destroys the inversion symmetry existing in the D_{3d} point group allowing some even and odd parity orbitals of the same multiplicity to mix, forming bonding-antibonding pairs with respect to the primitive orbitals of the D_{3d} conformation.

As it has already been pointed out, much information about the role played by individual orbitals on the origin of the instability of the D_{3d} structure can be obtained by calculating the force constant values K_I for the α_{2u} distortion corresponding to different electronic configurations I. Values of K_I obtained by means of DFT-B3LYP/TZP calculations in the high-symmetry D_{3d} structure for several configurations involving the orbitals displayed in Fig. 3 are shown in Table II. It is worth noting that although DFT-B3LYP calculations lead to values of the energy barrier that are about half of those obtained at QCISD and MP4 levels of theory, however, this method is well suited to analyze the microscopic origin of the barrier in a semiquantitative way.

In the ground state the calculated value is $K_{GS} = -5.64$ eV/Å^2. Seeking to clear out the origin of their instability, a model has been developed in order to estimate the K_0 and K_v^{ij} contributions to the force constant of the ground state, K_{GS}. First, the force constant K_I along the α_{2u} distortion for a given electronic configuration I is written as a function of K_0, the orbital contributions K_v^{ij}, and occupation numbers $n_i^{(i)}$ through Eq. (6). In the present model, the sum in Eq. (6) is extended to all pair of coupled i-j orbitals depicted in Fig. 3 with the exception of the deepest $1a_{1g}$ and

TABLE II. Calculated values of the force constants K_I (in eV/Å^2) for the α_{2u} distortion corresponding to the ground state (GS) and several excited electronic configurations I, denoted as one-electron excitations from the GS. Calculations were carried out at the DFT-B3LYP/TZP level of theory for the reference D_{3d} structure of $N_2H_7^+$.

Excitation	K_I
GS	−5.68
$3a_{1g} \rightarrow 4a_{1g}$	33.02
$3a_{1g} \rightarrow 4a_{2u}$	63.92
$3a_{1g} \rightarrow 2e_u$	23.84
$3a_{1g} \rightarrow 2e_g$	53.96
$3a_{1g} \rightarrow 5a_{1g}$	33.98
$1e_u \rightarrow 2e_u$	13.40
$1e_u \rightarrow 2e_g$	9.00
$3a_{2u} \rightarrow 4a_{1g}$	−10.24
$3a_{2u} \rightarrow 4a_{2u}$	−8.72
$3a_{2u} \rightarrow 2e_u$	−6.92
$3a_{2u} \rightarrow 2e_g$	−11.96
$3a_{2u} \rightarrow 5a_{1g}$	−0.84

$2a_{1g}$ levels whose contribution is assumed to be negligible. In a second step, the values of K_I calculated for the different electronic configurations (Table II) has been fitted to the previous model expression of K_I by means of a least squares procedure. The values of the vibronic contributions K_v^{ij} and their participation in K_{GS} are shown in Table III. The fit produces a value for K_0 equal to 99.52 eV/Å^2. Adding all contributions a value $K_{GS} = -5.85$ eV/Å^2 is obtained, in reasonable agreement with the B3LYP/TZP calculated one (−5.68 eV/Å^2).

We can now compare our results with those of other well established models in this field. Most usually the origin of the HB has been associated to the classical attraction associated with effective charges and dipole moments localized over polarized atoms (see Ref. 29 and references therein). However, many experimental and theoretical results in HBs indicate the existence of non-negligible covalent effects.[29,47] This feature is particularly important in strong HBs of the type covered by this study.[48] One representative model is the three-center-four-electron (3c-4e) one originally introduced

TABLE III. Value of K_v^{ij} (in eV/Å^2) and the corresponding $(n_i^{(I)} - n_j^{(I)}) K_v^{ij}$ contributions to the vibronic part K_v of GS force constant for couplings among i-j orbitals. Values of K_v^{ij} were obtained obtained by fitting the force constant data Table II with the model expression (7) through a mean square procedure. $n_i^{(I)}$ is the ocupation number of orbital i (with energy ε_i) in state I. Orbital energy differences $\Delta_{ij}^{(I)} = \varepsilon_i^{(I)} - \varepsilon_j^{(I)}$ (in eV) are also given.

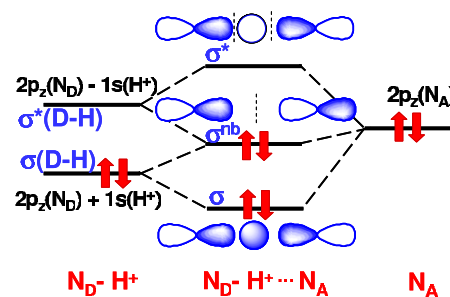| Coupling	K_v^{ij}	$(n_i^{(I)} - n_j^{(I)}) K_v^{ij}$	$\Delta_{ij}^{(I)}$
$3a_{1g}$-$3a_{2u}$	−24.64	0.0	7.00
$3a_{1g}$-$4a_{2u}$	−14.62	−29.24	22.50
$3a_{2u}$-$4a_{1g}$	−7.03	−14.06	14.50
$3a_{2u}$-$5a_{1g}$	−7.38	−14.76	16.60
$4a_{1g}$-$4a_{2u}$	−4.48	0.0	1.00
$4a_{2u}$-$5a_{1g}$	−0.35	0.0	1.10
$1e_u$-$1e_g$	−4.88	0.0	0.30
$1e_u$-$2e_g$	−6.11	−24.44	23.10
$1e_g$-$2e_u$	−5.67	−22.68	22.0
$2e_g$-$2e_u$	−3.23	0.0	0.80

FIG. 4. (Color online) Simple application of the Rundle–Pimentel three-center four-electron model to the N_D–$H^+ \cdots N_A$ SSHB of the proton-bound ammonia dimer cation $N_2H_7^+$.

by Pimentel and Rundle[27] to explain bonding in hypervalent molecules. Later, Coulson used a similar three-orbital-four-electron model employing VB theory to describe HB.[28] Also, Warshel and Weiss[31] implemented an empirical valence-bond (EVB) method to study reactions in solutions. This model allows one to estimate the covalent character of the HB both in gas and condensed phases and is extensively[10] used to study reactions in biological systems. Short-strong-hydrogen-bond (SSHB) have been interpreted[26] through a dative covalent (or electron donor-acceptor) bonding arising from an interaction between the doubly occupied p_σ orbital of the proton acceptor A and the σ^* lowest unoccupied molecular orbital (LUMO) of the proton donor fragment D–H, as depicted in Fig. 4. These interactions give rise to both $D \leftarrow A$ CT and weakening of the D–H bond through partial occupation of the σ^*(D–H) orbital.[29,30] In our model, the same picture can be obtained observing how the σ^{nb} orbital mixes with σ^* due to vibronic coupling.

Let us compare now the results from our model with those of the 3c-4e one.[25,26] Using Eq. (6) we can write the force constant for the ground state as

$$K_{GS} = K_0 - 2K_v^{3a_{1g}-4a_{2u}} - 2K_v^{3a_{2u}-4a_{1g}} - 2K_v^{3a_{2u}-5a_{1g}}$$
$$- 4K_v^{1e_u-2e_g} - 4K_v^{1e_g-2e_u}. \tag{7}$$

The numerical value of the constants in Eq. (7) can be found in Table III. In the 3c-4e of Rundle and Pimentel only σ-orbitals ($3a_{1g}, 3a_{2u}, 5a_{1g}$) are involved which, according to Table III, are the ones that have larger K_v values. In fact, the $3a_{1g}$ and $3a_{2u}$ are those more strongly coupled. However, strong coupling does not always imply a large influence in the distortion. It is worth noting that the $3a_{1g}$-$3a_{2u}$ coupling is not involved in the instability of the ground state [no term of this type appears in Eq. (7)] because both orbitals are fully occupied. In our vibronic model the main source of instability comes from the interaction of the $3a_{1g}$-$4a_{2u}$ orbitals [second term in Eq. (7), with a value of −29.2 eV/Å^2]. This large value can be clearly correlated with the force constants calculated in Table II since the one corresponding to the $3a_{1g}$-$4a_{2u}$ excitation is the largest that we have calculated. It is also important to note that the $4a_{2u}$ orbital, whose wavefunction largely corresponds to the hydrogen atoms forming part of the ammonia molecules, is not present in the Rundle–Pimentel model. Also, and again at difference with the 3c-4e model in Eq. (7), the e-type orbitals also contribute to the instability [two last terms in Eq. (7)]. Due to the smaller σ
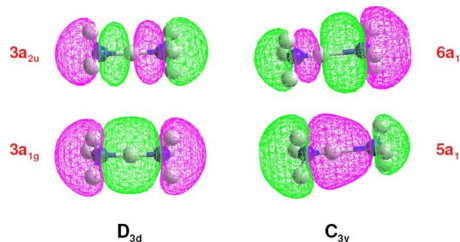
FIG. 5. (Color online) Variation in charge distribution for $3a_{1g}$ and $4a_{2u}$ orbitals when $N_2H_7^+$ is distorted from D_{3d} to C_{3v} symmetry.

FIG. 6. (Color online) Comparison between the molecular orbital diagrams of D_{3d} $N_2H_7^+$ and D_{2d} $H_5O_2^+$ molecules as obtained from MP4/6311++G** calculations. Level energies are given in eV units. Contour plots of high-lying occupied orbitals are also shown. Contour values correspond to density of charge values of 0.01.

character, the coupling between these orbitals is much weaker [about three to six times (Table III)] than between *a*-type orbitals. However, *e*-type orbitals can be occupied by twice the number of electrons than *a*-type ones which partly compensates this lack of coupling. Adding all *a*-type contributions (mainly with σ character) and *e*-type contributions (mainly π character) we find that the former (-58.1 eV/Å^2) is more important than the latter (-47.1 eV/Å^2), in agreement with the Rundle–Pimentel model.[26,27] However, the contribution coming from *e*-orbitals is significant and if neglected $N_2H_7^+$ would not have instability along the α_{2u} mode.

In Fig. 5 it can be seen that vibronic coupling favors the accumulation of charge over the donor for $3a_{1g}$ and over the acceptor for $3a_{2u}$. A similar picture including also the *e*-type orbitals (Fig. 2 in the supplemental information) shows that $1e_u$ and $1e_g$ orbitals accumulate charge over donor and acceptor, respectively. The vibronic contributions that favor accumulation of charge over donor and acceptor are nearly compensated suggesting that the net electron CT has to be very small. Since the sum of vibronic contributions for $3a_{1g}$ and $1e_u$ is slightly larger than that for $3a_{2u}$ and $1e_g$ the small CT occurs in the $D \leftarrow A$ direction, in agreement with previous studies[29,30] and also the EVB approach when no solvent is introduced.[31]

Recently Martín-Pendás *et al.*[30] performed a detailed analysis of the energetic terms of various dimers covering from weak to strong HB extremes and comparing different decomposition schemes. They showed that both electrostatic and covalent views of the HB are compatible, recovering one or the other picture depending on how one defines the different energy terms. According to Bersuker,[22] PJT contributions to K_v can also be divided into two classes: Polarization terms coming from coupled orbitals that belong to the same atom, and covalent terms that relate orbitals coming from different atoms. Using this classification one could conclude that most of the PJT contributions described above are covalent as describe the interaction of occupied orbitals with a large nitrogen character with unoccupied ones that have H character. However, this classification is not adequate in a HB system where the terms polarization and covalence are applied to molecular fragments rather than to individual atoms. In order to discuss this subject, we will use PJT covalent terms to those that relate one orbital of the proton with another coming from a NH$_3$ fragment and PJT polarization terms to those that only involve NH$_3$ fragments. This means that polarization is referred here to the NH$_3$ molecule as a whole. This implies that the $3a_{2u}$-$5a_{1g}$ coupling is a covalent term, while
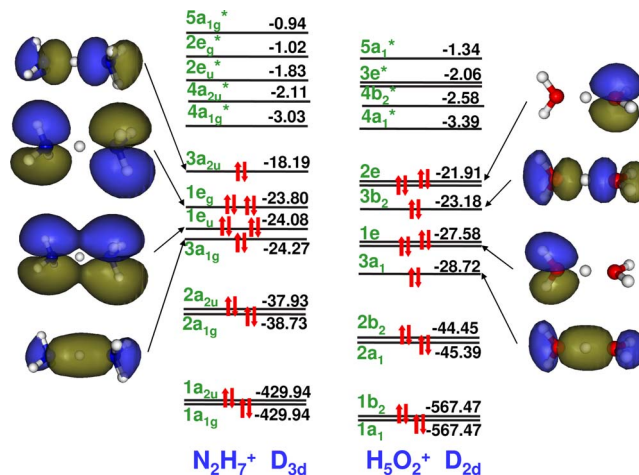
$3a_{2u}$-$4a_{1g}$, $1e_u$-$2e_g$, $1e_g$-$2e_u$ are polarization ones and $3a_{1g}$-$4a_{2u}$ has a mixed character. Using this definition and the data in Table III we find that polarization terms dominate over covalent ones. In this sense, our results are in agreement with those obtained from the EVB model[31] where more information can be extracted with the inclusion of solvent effects that results in reinforced polarization terms.[49] However, it is important to note that since the covalent term contribution to the force constant is larger than K_{GS} (in absolute value), the instability will be destroyed if we neglect them. One could also argue that the way we have defined the polarization terms here represents the change in the *shape* of the electron density around the NH$_3$ fragments as we go from the D_{3d} configuration to the C_{3v} one and, as a consequence, also represents a change in the covalence of the bonds. Thus, we conclude that the importance of polarization and covalent terms in this case is largely a matter of how one partitions the electron density and its redistribution upon distortion, in agreement with the analysis carried out by Martín-Pendás *et al.*[30]

E. Differences between $N_2H_7^+$ and $H_5O_2^+$

In contrast with $N_2H_7^+$, the proton is located midway between both oxygen atoms in the ground state configuration of $H_5O_2^+$ (C_2 symmetry). We can explore the vibronic coupling differences between both systems using the analogous high-symmetry D_{2d} configuration in $H_5O_2^+$ since the C_2 geometry corresponds to a small deformation of the D_{2d} one which is not relevant in the present analysis. At B3LYP and MP4 levels of theory, the D_{2d} configuration of $H_5O_2^+$ is stable under the b_2 vibration involving the proton-transfer movement. The value of K_{GS} is $+4.05$ eV/Å^2. In Fig. 6 the orbital schemes of D_{3d} $N_2H_7^+$ and D_{2d} $H_5O_2^+$ molecules are compared. The main difference existing between them is that the highest occupied molecular orbital (HOMO) in $N_2H_7^+$ ($3a_{2u}$) is a nondegenerate orbital that has a σ character while in $H_5O_2^+$ it is a doubly degenerate *e*-orbital of π-type for the O–H$^+$–O bond.

TABLE IV. Comparison of the vibronic contributions to the GS force constant K_{GS} along the proton off-center movement for D_{3d} N$_2$H$_7^+$ and D_{2d} H$_2$O$_5^+$ molecules. K_0 is the primary force constant, and $K_v^{(\sigma)}$ and $K_v^{(\pi)}$ are respectively the sum of K_v^{ij} contributions for σ and π-type bonding orbitals. All K values are given in eV/Å^2.

System	K_{GS}	K_0	$K_v^{(\sigma)}$	$K_v^{(\pi)}$	$K_v^{(\sigma)}/K_0$	$K_v^{(\pi)}/K_0$
N$_2$H$_7^+$	−5.6	99.5	58.1	47.1	0.58	0.47
H$_5$O$_2^+$	4.1	126.3	86.9	35.1	0.69	0.28

In Table IV we compare the main vibronic contributions to the $\alpha(a_{2u})$ proton-transfer distortion in N$_2$H$_7^+$ and H$_5$O$_2^+$. We can see that in the latter molecule all the vibronic constants (both K_0 and K_v^{ij}) are larger than those in the former. However, the PJT effect is not strong enough to overcome the elastic barrier represented by K_0 and the distortion does not occur. Moreover, it can be seen in Table IV that the contributions with π character (coming from e-e couplings) in H$_5$O$_2^+$ are weaker than the corresponding ones (e_g-e_u couplings) in N$_2$H$_7^+$. The main reason for this difference is that the lone pairs (Fig. 7) of the water molecules in H$_5$O$_2^+$ are orthogonal to the proton displacement, participating very little in the formation of new O−H$^+$ bonds. On the other hand, in N$_2$H$_7^+$ the e-type orbitals are slightly angled (Fig. 7) and participate more in bounding the proton.

The D_{2d} configuration of H$_5$O$_2^+$ is unstable with respect to b_1- and e-type vibrations, their frequencies at the MP2(B3LYP)/6-31G* levels being, respectively, 314i (268i) cm^{-1} and 572i (517i) cm^{-1}. These two instabilities lead, respectively, to the C_2 and C_s stationary points of the APES (Fig. 5). b_1-type vibrations do not bend the O−H$^+$−O bond and, as a consequence, the lone pairs remain perpendicular to the H$^+$ off-center motion. Therefore, in the C_2 configuration the proton is equidistant to both oxygen atoms. However, following e-distortions (Fig. 2) the O−H$^+$−O bond is bent increasing the PJT contributions associated to the e orbitals. This leads to the off-center motion of the proton and to the formation of one long and one short O−H bond in the C_s configuration of H$_5$O$_2^+$.

F. Quantum vibrational dynamics

As it was previously indicated, the existence of a double-well APES (instability of the static D_{3d} structure) in N$_2$H$_7^+$ is accompanied with a large change in the N−N distance. Therefore, the existence of a LBHB and the special proton dynamics in N$_2$H$_7^+$ may be related to this coupling between the α_{2u} and α_{1g} vibrational modes (Fig. 1). Asada $et\ al.$[15] were the first to perform dynamical calculations in this system. Multidimensional calculations of the dynamics of a molecule are very time consuming and computationally demanding. For this reason, Asada $et\ al.$[15] only considered an average of the α_{2u}-α_{1g} modes. On the other hand, Asmis $et\ al.$[17] performed a joint experimental-theoretical work where they obtained the N$_2$H$_7^+$ infrared spectrum and simulated it using a four-dimensional energy surface. In both works the APES was calculated at the MP2 level of theory. In Sec. III A we have already seen that MP2 calculations lead to an important underestimation ($\sim$45%) of the barrier when compared to the more accurate MP4 or QCISD methods. Thus, we set to calculate the vibrational levels of N$_2$H$_7^+$ at the MP4/6-311++G** level taking into account the two modes that we have found to be more strongly coupled, α_{2u} and α_{1g} as a result of anharmonicity. Selecting these two modes, it is not only physically significant but also allows to dramatically reduce the computational effort (see computational details).

The $E[Q(\alpha_{2u}), Q(\alpha_{1g})]$ APES calculated at the MP4/6-311++G** level is shown in the first picture of Fig. 8. The saddle point of this APES, situated at the origin
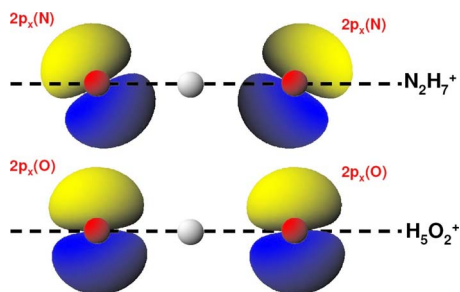

FIG. 7. (Color online) Schematic picture showing the different positions of the 2p_x orbitals of N and O atoms participanting in the e-type molecular orbitals (with π character) in D_{3d} N$_2$H$_7^+$ and D_{2d} H$_5$O$_2^+$ molecules, respectively.
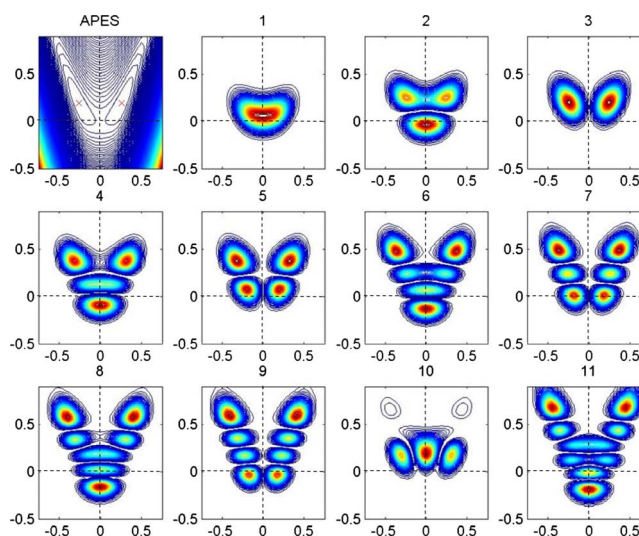

FIG. 8. (Color online) Bidimensional $[Q(\alpha_{2u}), Q(\alpha_{1g})]$ APES computed at the MP4/6-311++G** level of theory, and representation of densities of probability of appareance for the first 11 vibrational states as function of $Q(\alpha_{2u})$ (x axis) and $Q(\alpha_{1g})$ (y axis) normal coordinates (in Å units). The origin of coordinates corresponds to the transition state D_{3d} symmetric structure, while the two equivalent C_{3v} minima of the APES are denoted by red crosses.

(0,0), corresponds to the transition state D_{3d} structure, while the two equivalent minima are related to the C_{3v} structures with $(\pm 0.26, 0.19)$ Å coordinates. It is worth noting the asymmetry existing between the positive and negative $Q(\alpha_{1g})$ directions of the APES. Going along the positive $Q(\alpha_{1g})$ axis (that is, increasing the R distance between both NH_3 groups with respect to the optimized value for the transition state structure) gives rise to a deeper double-well APES in $Q(\alpha_{2u})$. It is also interesting to note that moving in the APES along the $Q(\alpha_{1g})=0$ line (that is, keeping fixed the R distance at the optimized value for the transition state

structure), a double-well is found although the energy barrier is smaller than the one found at the $Q(\alpha_{1g})$ value corresponding to the optimized minima.

The shape of this bidimensional APES can be understood by means of a simple model that considers the PJT coupling of the ground state with only one appropriate excited state through both α_{2u} and α_{1g} modes but considering that the geometry of the transition D_{3d} structure for the excited state is different to that corresponding to the ground state. The linear vibronic matrix corresponding to this PJT coupling model can be written as

$$\begin{pmatrix} -\Delta + \frac{1}{2}K(\alpha_{2u})Q(\alpha_{2u})^2 + \frac{1}{2}K(\alpha_{1g})Q(\alpha_{1g})^2 & F(\alpha_{2u})Q(\alpha_{2u}) \\ F(\alpha_{2u})Q(\alpha_{2u}) & \Delta + \frac{1}{2}K(\alpha_{2u})Q(\alpha_{2u})^2 + \frac{1}{2}K(\alpha_{1g})Q(\alpha_{1g})^2 - F(\alpha_{1g})Q(\alpha_{1g}) \end{pmatrix}, \tag{8}$$

where $K(\alpha_{2u})$ and $K(\alpha_{1g})$ are the primary force constants along α_{2u} and α_{1g} modes, respectively, Δ is the excitation energy, $F(\alpha_{2u})$ is the PJT linear coupling constant, and $F(\alpha_{1g})$ is the force along $Q(\alpha_{1g})$ in the excited state for the transition D_{3d} structure. Diagonalizing Eq. (8) we obtain the following energies

$$\varepsilon_{\pm} = \frac{1}{2}K(\alpha_{2u})Q(\alpha_{2u})^2 + \frac{1}{2}K(\alpha_{2u})Q(\alpha_{2u})^2 + \frac{1}{2}F(\alpha_{1g})Q(\alpha_{1g}) \pm \frac{1}{2}\sqrt{4(F(\alpha_{2u})Q(\alpha_{2u}))^2 + (F(\alpha_{1g})Q(\alpha_{1g}) + 2\Delta)^2}. \tag{9}$$

A Taylor expansion of Eq. (9) reveals that the leading cubic anharmonic contributions ($\gamma = -F(\alpha_{2u})^2 F(\alpha_{1g})Q(\alpha_{2u})^2 Q(\alpha_{1g})/4\Delta^3$) contains important cross-mode coupling terms that render the harmonic approximation invalid and make both modes nonseparable. From Eq. (9) two relevant consequences can be easily obtained. On one hand, the depth of the double-well along $Q(\alpha_{2u})$ is directly related to the magnitude of the $Q(\alpha_{1g})$ coordinate. On the other hand, after performing some algebra, we obtain the following condition for the appearance of a double-well along the $Q(\alpha_{2u})$ coordinate:

$$\frac{F(\alpha_{2u})^2}{K(\alpha_{2u})} > \Delta - \frac{1}{2}F(\alpha_{1g})Q(a_{1g}). \tag{10}$$

Within this model the coupling between a $Q(\alpha_{1g})$ mode and a mode of other symmetry can only take place if the relaxed geometry in the considered excited state is displaced along the $Q(\alpha_{1g})$ coordinate with respect to the one in the ground state. This can be induced from the experimental evidence[25,50] that the Stokes shift of the luminescence peaks has always a significant contribution from the fully symmetrical α_{1g} mode, revealing a displacement along this mode in the excited states. In the case of $N_2H_7^+$ an important diminution of the N–N distance (compression along the α_{1g} mode) of about 15 pm has been obtained by means of DFT-GGA calculations when passing from the ground to the first excited state, corresponding to the HOMO $(a_{2u}) \rightarrow$ LUMO (a_{1g}) one-electron transition. It is worth noting that most PJT models do not consider the coupling of the α_{1g} mode with other modes of different symmetries despite the fact that it is responsible of relevant facts, as it has been shown in the case of $N_2H_7^+$.

The kind of coupling between α_{1g} and α_{2u} modes de-

scribed above can also be found in a model that considers mechanisms such as the dependency of the PJT constant with totally symmetric vibrations, different force constants along $Q(\alpha_{1g})$ in the ground and excited states, or cubic terms of the $Q(\alpha_{1g})Q(\alpha_{2u})^2$ type. Despite the well known fact that these mechanisms strongly affect the dynamics of the nuclear frame of any polyatomic system presenting a PJT,[17,23,51] there are few studies devoted to determine when each of these effects may be important in different molecules. Since they affect differently the vibronic matrix, they could lead to different diabatic behaviors in the dynamics. Thus, we suggest that the study of these effects may be important when other borderline PJT cases are considered.

The vibrational states associated to this bidimensional ground state APES were obtained by solving the corresponding stationary Schrödinger equation. The energies of first 14 levels are given in Table V, while their nuclear densities are depicted in Fig. 8. Levels in Table V are labeled using an independent (harmonic) mode notation, $|v(\alpha_{2u})v(\alpha_{1g})\rangle$, where $v(i)=0,1,\ldots$ indicates the level of excitation of mode $i=\alpha_{2u}, \alpha_{1g}$. However, this notation is only approximate as it does not consider mixing between vibrational states of the same symmetry. The $E(v_{a1g})$ column in Table I shows the vibrational energies calculated using the cross section of the APES when $Q(\alpha_{2u})=0$. These levels are significantly shifted when compared to the ones corresponding to the same excitation in the two-dimensional APES. Another important difference is that the energy of the $|2\,0\rangle$ state is much larger than the one expected from an independent-mode model because this state is strongly mixed with all the states of A_{1g} symmetry with lower energy.

The maximum of nuclear density at the vibrational ground state (state 1 in Fig. 8) corresponds to a centro-

TABLE V. Energies $E_{\nu(\alpha_{2u})\nu(\alpha_{1g})}$ of the first 14 vibrational levels corresponding to the bidimensional $[Q(\alpha_{2u}),Q(\alpha_{1g})]$ APES calculated at the MP4/6-311++G** level of theory. Energies are given with respect to the GS $\nu(\alpha_{2u})=0$ $\nu(\alpha_{1g})=0$ level (ZPE). We also show the assignment of the experimental infrared spectra taken from the work of Asmis *et al.* (Ref. 16). All energies are given in cm^{-1}.

Level	$\nu(\alpha_{2u})$	$\nu(\alpha_{1g})$	$E_{\nu(\alpha_{2u})\nu(\alpha_{1g})}$	E_{expt}	Symmetry
1	0	0	0		a_{1g}
2	0	1	430		a_{1g}
3	1	0	451		a_{2u}
4	0	2	804		a_{1g}
5	1	1	832	743 (A)	a_{2u}
6	0	3	11.57		a_{1g}
7	1	2	1199	1097 (C)	a_{2u}
8	0	4	1496		a_{1g}
9	1	3	1545	1451 (F)	a_{2u}
10	2	0	1744		a_{1g}
11	Not assigned	Not assigned	1817		a_{1g}
12	1	4	1866		a_{2u}
13	0	6	2097		a_{1g}
14	1	5	2156		a_{2u}

symmetric D_{3d} geometry, $Q(\alpha_{2u})=0$, where $Q(\alpha_{1g})=0.06$ Å, that is, the N–N distance is much greater ($R=2.596$ Å) than at the transition D_{3d} structure of the APES, while N–H distances and H–N–H$^+$ angles of NH$_3$ units only experience small increase. The maximum is very flat along the $Q(\alpha_{2u})$ direction reflecting the existence of the double-well APES while the probability rapidly decays when the distance R between the NH$_3$ units increases. The heart-shaped vibrational ground state density (Fig. 8) is another consequence of the nonseparability of the two modes. Although this state is denoted as $|0\ 0\rangle$ in Table I, its wavefunction is a mix of $|0\ 0\rangle$ with all functions of A_{1g} symmetry, particularly with the $|2\ 1\rangle$ state (which is not shown in Table V and Fig. 8 because of its high energy).

In Table V we also show the assignment of the experimental infrared spectra taken from the work of Asmis *et al.*[17] In our dynamical calculations the only infrared-active vibrational states are those that have a_{2u} symmetry. Then, we can assign bands A, C and F measured by Asmis *et al.*[17] to the transitions (all allowed by symmetry) from the ground state to $|1\ 1\rangle$, $|1\ 2\rangle$, and $|1\ 3\rangle$ excited states, respectively, in our bidimensional surface. To assign the rest of the spectrum we perform a vibrational (harmonic) calculation in D_{3h} N$_2$H$_7^+$, where the N–N distance has been adjusted to that of the maximum of nuclear density of the ground state in our dynamical simulation. According to this calculation, we can assign bands D (1325 cm^{-1}) and G (1545 cm^{-1}) measured by Asmis *et al.*[17] to modes a_{2u} (1362 cm^{-1}) and e_u (1605 cm^{-1}), respectively. Band D corresponds to umbrella-inversion movement in agreement with the study of Asmis *et al.*[17] In their 4D dynamic calculations the frequency is slightly red-shifted to 1354 cm^{-1} which seems a slight improvement at the cost of a large increase in the computational cost of the calculation. We can also tentatively assign band B (938 cm^{-1}) to a transition where both the proton-transfer mode, a_{2u} ($\sim$400 cm^{-1}), and the symmetric NH$_3$ tilting (with respect to the axis of the molecule) mode, e_g (665 cm^{-1}), are excited to their first excited state. The resulting mode has the

correct symmetry to be IR-active (e_u) and is also a good candidate to produce an appreciable coupling between both modes because the e_g-mode distorts the σ-bonding in the N–H–N direction which, according to our results of Sec. III D and III E, it is crucial to get an instability that allows proton transfer. Then, we obtain satisfactory results where we can assign most experimental modes by performing a dynamical calculation only in a bidimensional surface and a common harmonic frequency calculation. Qualitative arguments associated with the vibronic analysis support our assignment.

IV. CONCLUSIONS

In this work we have studied the origin of the LBHB in the N$_2$H$_7^+$ cation (that has a double-well APES) using PJT theory and used these results to compare this molecule with H$_5$O$_2^+$, having a single-well APES. To the best of our knowledge, this is the first time that a quantitative PJT analysis has been used to study a proton transfer, and it reveals many details that will prove useful to understand other HB molecules. In this sense, it is worth noting that the present study of proton transfer in N$_2$H$_7^+$ has been carried out using a similar PJT analysis that the ones previously performed in the case of on-center[43] and off-center[24,25] instabilities of transition metal impurities in fluorite-type crystals. Rebonding effects (formation of new covalencies) due to PJT vibronic couplings are responsible for the high symmetry instabilities in all that systems, although effects are much smaller in N$_2$H$_7^+$ where the energy barrier for the off-center displacement of the proton is very low.

In the first step we had to check the reliability of several *ab initio* and DFT methods. In agreement with the results found in literature, our calculations indicate that usual GGA exchange-correlation functionals provide inaccurate results while LDA leads to qualitatively wrong ones. The B3LYP hybrid functional performs better but there are still significant differences with more accurate *ab initio* results. Thus, caution must be taken when simulating hydrogen bonded

systems with these methods both in the single molecule regime or condensed phases.

Using a PJT model, we have shown that the main contribution to the off-center movement of the proton in $N_2H_7^+$ comes from the a_{1g}-a_{2u} coupling associated with the changes occurring in the three-center σ bonding along the $N-H^+-N$ axis. This represents a generalization of the 3c-4e Rundle–Pimentel and Coulson models. However, we also find additional contributions coming from π-type orbitals that are significant enough to destroy the instability if ignored. In fact, we can understand the absence of off-center displacement of the central proton in $H_5O_7^+$ due to the weaker π-type vibronic contribution in this system. Thus, the main difference existing between $N_2H_7^+$ and $H_5O_2^+$ (when discussing the off-center displacement of the proton) resides in the small tilting with respect to the $N-H^+-N$ axis of the π-orbitals with $2p(N)$ character that is not present in the $2p(O)$ ones in $H_5O_2^+$.

Our model has also allowed us to study the CT occurring during the formation of the hydrogen bond and the contribution of covalent and polarization effects. In the first subject, we find that vibronic contributions, which favor accumulation of charge over donor and acceptor N atoms, are nearly compensated suggesting that the net electron CT in the D $\leftarrow$ A direction has to be very small, in agreement with previous studies.[29,30] On the second point, we have concluded, in a similar way to Martín-Pendás *et al.*,[30] that the relative covalent and polarization contributions depend on how one arbitrarily partitions the electron density and its redistribution upon distortion. Thus, if one partitions the charge in a similar way as proposed by EVB models, we find that polarization terms are dominant while if one uses the criteria usually employed in PJT theory covalent ones are dominant.

Finally, we have carried out a bidimensional study of the $N_2H_7^+$ quantum dynamics on the $\{Q(\alpha_{2u}), Q(\alpha_{1g})\}$ plane. We have shown that the vibrational frequencies can be understood when the coupling between these modes is included and the rest are considered under the harmonic approximation. We propose that this coupling comes from the differences existing in the N–N distance in the ground state and the excited one which is PJT coupled to it.

ACKNOWLEDGMENTS

[1] R. P. Bell, *The Proton in Chemistry* (Cornell University Press, Ithaca, New York, 1973); *Proton Transfer Reactions* edited by E. Caldin and V. Gold (Wiley, New York, 1975); *Ultrafast Hydrogen Bonding Dynamics and Proton Transfer Processes in the Condensed Phase*, edited by T. Elsaesser and H. J. Bakker (Kluwer, Dordrecht, 2002); C. Tanner, C. Manca, and S. Leutwyler, Science **302**, 1736 (2003); M. Iannuzzi and M. Parrinello, Phys. Rev. Lett. **93**, 025901 (2004); O. F. Mohammed, D. Pines, J. Dreyer, E. Pines, and E. T. J. Nibbering, Science **310**, 83 (2005); J. T. Hynes, Nature (London) **446**, 270 (2007); *Hydrogen-Transfer Reactions*, edited by J. T. Hynes, J. P. Klinman, H.-H. Limbach, and R. L. Schowen (Wiley-VCH, Weinheim, 2007) Vols 1–4.

[2] M. Krishnamurthy, J. A. de Gouw, L. N. Ding, V. M. Bierbaum, and S. R. Leone, J. Chem. Phys. **106**, 530 (1993); S. Hamon, T. Speck, J. B. A. Mitchell, and B. R. Rowe, *ibid.* **117**, 2557 (2002); M. A. Smith, in *Unimolecular and Biomolecular Ion-Molecule Reaction Dynamics*, edited by C.-Y. Ng, T. Baer, and I. Powis (Wiley, New York, 1992), p. 183.

[3] V. W. Weiss and W. H. Flygare, J. Chem. Phys. **45**, 8 (1996).

[4] L. Rosso and M. Tuckerman, Solid State Ionics **161**, 219 (2003).

[5] H. J. Berthold, E. Vonholdt, R. Wartchow, and T. Vogt, Z. Kristallogr. **203**, 199 (1993).

[6] A. Zecchina, L. Marchese, S. Bordiga, C. Pazè, and E. Gianoti, J. Phys. Chem. B **101**, 10128 (1997).

[7] A. Micek-Ilnicka and B. Gil, Vib. Spectrosc. **43**, 435 (2007).

[8] J. L. Atwood, L. J. Barbour, and A. Jerga, J. Am. Chem. Soc. **124**, 2122 (2002).

[9] X.-J. Song and A. E. McDermott, Magn. Reson. Chem. **39**, S37 (2001).

[10] A. Warshel and A. Papazyan, Proc. Natl. Acad. Sci. U.S.A. **93**, 13665 (1996); C. N. Schutz and A. Warshel, Proteins **55**, 711 (2004).

[11] J. M. Price, M. W. Crofton, and Y. T. Lee, J. Phys. Chem. **95**, 2182 (1991).

[12] P. Merlet, S. D. Peyerimhoff, and R. J. Buenker, J. Am. Chem. Soc. **94**, 8301 (1972); J. J. Delpuech, G. Serratrice, A. Strich, and A. Veillard, J. Chem. Soc., Chem. Commun.817 (1972); K. Hirao, T. Fujikawa, H. Konishi, and S. Yamabe, Chem. Phys. Lett. **104**, 184 (1984); J. E. Del-Bene, M. J. Frisch, and J. A. Pople, J. Phys. Chem. **89**, 3669 (1985); B.-C. Wang, J.-C. Chang, J.-C. Jiang, and S.-H. Lin, Chem. Phys. **276**, 93 (2002); M. Pecul, J. Sadlej, and T. Helgaber, Chem. Phys. Lett. **372**, 476 (2003).

[13] S. Scheiner, J. Chem. Phys. **75**, 5791 (1981); **77**, 4039 (1982).

[14] J. A. Platts and K. E. Laidig, J. Phys. Chem. **99**, 6487 (1995); **100**, 13455 (1996); B. S. Jursic, J. Mol. Struct.: THEOCHEM **393**, 1 (1997); L. W. Barich, J. B. Nicholas, and J. F. Haw, J. Phys. Chem. A **105**, 4708 (2001); M. Meuwly and M. Karplus, J. Chem. Phys. **116**, 2572 (2002).

[15] T. Asada, H. Haraguchi, and K. Kitaura, J. Phys. Chem. A **105**, 7423 (2001).

[16] M. E. Tuckerman, D. A. Yarne, S. O. Samuelson, L. A. Hughes, and G. J. Martyna, Comput. Phys. Commun. **128**, 333 (2000); Y. Liu and M. E. Tuckerman, J. Phys. Chem. B **105**, 6598 (2001).

[17] K. R. Asmis, Y. Yang, G. Santambrogio, M. Brümmer, J. R. Roscioli, L. R. Cunn, M. A. Johnson, and O. Kühn, Angew. Chem., Int. Ed. **46**, 8691 (2007).

[18] D. Marx, ChemPhysChem **7**, 1848 (2006).

[19] B. Kichner, ChemPhysChem **8**, 41 (2007).

[20] K. R. Asmis, N. L. G. Santambrogio, M. Brümmer, C. Kaposta, D. M. Neumark, and L. Wöste, Science **299**, 1375 (2003); T. D. Fridgen, T. B. McMahon, L. MacAleese, J. Menaire, and P. Maitre, J. Phys. Chem. A **108**, 9008 (2004); J. Sauer and J. Döbler, ChemPhysChem **6**, 1706 (2005); J. M. Headrik, E. G. Dicken, R. S. Walters, N. I. Hammer, R. A. Christie, J. Cui, E. M. Myshakin, M. A. Duncan, M. A. Johnson, and K. D. Jordan, Science **308**, 1765 (2005); T. James and D. J. Wales, J. Chem. Phys. **122**, 134306 (2005).

[21] E. G. Dicken, J. M. Headrick, J. R. Roscoli, J. C. Bopp, M. A. Johnson, and A. B. McCoy, J. Phys. Chem. A **109**, 1487 (2005); Y. Xie, R. B. Remington, and H. F. Schaefer III, J. Chem. Phys. **101**, 4878 (1994); P. L. Plummer, J. Phys. Chem. B **101**, 6251 (1997); E. F. Valeev and H. F. Schaefer III, J. Chem. Phys. **108**, 7197 (1998); S. Sadhukhan, D. Muñoz, C. Adamo, and G. E. Scuseria, Chem. Phys. Lett. **306**, 83 (1999); A. L. Sobolewski and W. Domcke, J. Phys. Chem. A **106**, 4158 (2002); X. Huang, H. M. Cho, S. Carter, L. Ojamäe, J. M. Bowman, and S. J. Singer, *ibid.* **107**, 7142 (2003); X. Huang, B. J. Braams, and J. M. Bowman, J. Chem. Phys. **122**, 044308 (2005); M. V. Vener and J. Sauer, Phys. Chem. Chem. Phys. **7**, 258 (2005).

[22] I. B. Bersuker, *The Jahn-Teller effect* (Cambridge University Press, London, 2006).

[23] H. Köppel, W. Domcke, and L. S. Cederbaum, Adv. Chem. Phys. **57**, 59 (1984).

[24] P. García-Fernández, J. A. Aramburu, M. T. Barriuso, and M. Moreno, Phys. Rev. B **69**, 174110 (2004); **73**, 184122 (2006).

[25] M. Moreno, M. T. Barriuso, J. A. Aramburu, P. García-Fernández, and J. M. García-Lastra, J. Phys.: Condens. Matter **18**, R315 (2006).

[26] G. A. Landrum, N. Goldberg, and R. Hoffmann, J. Chem. Soc. Dalton Trans. **1997**, 3605.

[27] G. C. Pimentel, J. Chem. Phys. **19**, 446 (1951); R. J. Hackand and R. E. Rundle, J. Am. Chem. Soc. **73**, 4321 (1951).

[28] C. A. Coulson and U. Danielsson, Ark. Fys. **8**, 239 (1954).

[29] I. V. Alabugin, M. Manoharan, S. Peabody, and F. Weinhold, J. Am. Chem. Soc. **125**, 5973 (2003); A. van der Vaart and K. M. Merz, Jr., Int. J. Quantum Chem. **77**, 27 (2000); P. E. Frey, Magn. Reson. Chem. **39**, S120 (2001); P. Hobza and Z. Havlas, Chem. Rev. (Washington, D.C.) **100**, 4253 (2000); O. Gálvez, P. C. Gómez, and L. F. Pacios, J. Chem. Phys. **115**, 11166 (2001).

[30] A. Martín-Pendás, M. A. Blanco, and E. Francisco, J. Chem. Phys. **125**, 184112 (2006).

[31] A. Warshel and R. M. Weiss, J. Am. Chem. Soc. **102**, 6218 (1980).

[32] M. J. Frisch, G. W. Trucks, H. B. Schlegel *et al.*, GAUSSIAN 98, Revision A.9, Gaussian, Inc., Pittsburgh, PA, 1998.

[33] T. H. Dunning, Jr., J. Chem. Phys. **90**, 1007 (1989); R. A. Kendall, T. H. Dunning, Jr., and R. J. Harrison, *ibid.* **96**, 6796 (1992); D. E. Woon and T. H. Dunning, Jr., *ibid.* **98**, 1358 (1993).

[34] S. J. Vosko, L. Wilk, and M. Nusair, Can. J. Phys. **58**, 1200 (1980).

[35] J. P. Perdew, in *Electronic Structure of Solids '91*, edited by P. Ziesche and H. Eschrig (Akademie Verlag, Berlin, 1991), p. 11.

[36] A. D. Becke, Phys. Rev. A **38**, 3098 (1988); C. Lee, W. Yang, and R. G. Parr, Phys. Rev. B **37**, 785 (1988).

[37] A. D. Becke, J. Chem. Phys. **98**, 5648 (1993).

[38] G. te Velde, F. M. Bickelhaupt, E. J. Baerends, C. Fonseca Guerra, S. J. A. van Gisbergen, J. G. Snijders, and T. Ziegler, J. Comput. Chem. **22**, 931 (2001).

[39] B. Fornberg, SIAM Rev. **40**, 685 (1998).

[40] MATLAB 6.5, The MathWorks, Inc. 2002.

[41] N. Lopez and F. J. Illas, J. Phys. Chem. B **102**, 1430 (1998); M. T. Barriuso, J. A. Aramburu, and M. Moreno, J. Phys.: Condens. Matter **11**, L525 (1999).

[42] Y. Zhao and D. G. Truhlar, J. Phys. Chem. A **109**, 6624 (2005).

[43] B. Braïda, P. C. Hiberty, and A. Savin, J. Phys. Chem. A **102**, 7872 (1998); B. J. Lynch and D. G. Truhlar, *ibid.* **105**, 2936 (2001); **107**, 8996 (2003); G. Pacchioni, C. Di Valentin, D. Dominguez-Ariza, F. Illas, T. Bredow, T. Klüner, and V. Staemmler, J. Phys.: Condens. Matter **16**, S2497 (2004); Y. Zhao, B. J. Lynch, and D. G. Truhlar, J. Phys. Chem. A **108**, 2715 (2004); J. Ireta, J. Neugebauer, and M. Scheffler, *ibid.* **108**, 5692 (2004); Y. Zhao, N. González-García, and D. G. Truhlar, *ibid.* **109**, 2012 (2005); P. García Fernández, I. B. Bersuker, J. A. Aramburu, M. T. Barriuso, and M. Moreno, Phys. Rev. B **71**, 184117 (2005); P. García Fernández, C. Sousa, J. A. Aramburu, M. T. Barriuso, and M. Moreno, *ibid.* **72**, 155107 (2005); S. Shaik, D. Kumar, S. P. de Visser, A. Altun, and W. Thiel, Chem. Rev. (Washington, D.C.) **105**, 2279 (2005); S. Grimme, Angew. Chem., Int. Ed. **45**, 4460 (2006); A. Trueba, J. M. García-Lastra, C. de Graaf, P. García Fernández, M. T. Barriuso, J. A. Aramburu, and M. Moreno, Chem. Phys. Lett. **430**, 51 (2006).

[44] See EPAPS Document No. E-JCPSA6-129-619837 to see the optimized geometry of C_2 and C_s configurations of $H_5O_2^+$ at MP4(B3LYP)/aug-cc-pVTZ level as well as the vibrational frequencies at these geometries and tridimensional representations of the occupied and unoccupied orbitals of $N_2H_7^+$ at the C_{3v} minimum and D_{3d} transition state. For more information on EPAPS, see http://www.aip.org/pubservs/epaps.html.

[45] J. A. Pople, A. P. Scott, M. W. Wong, and L. Random, Isr. J. Chem. **33**, 345 (1993).

[46] P. Garcia-Fernandez, J. A. Aramburu, M. T. Barriuso, and M. Moreno, J. Chem. Phys. **128**, 124513 (2008).

[47] E. D. Isaacs, A. Shukla, P. M. Platzman, D. R. Hamann, B. Barbiellini, and C. A. Tulk, Phys. Rev. Lett. **82**, 600 (1999); G. Gilli and P. Gilli, J. Mol. Struct. **552**, 1 (2000); W. H. Thompson and J. T. Hynes, J. Am. Chem. Soc. **122**, 6278 (2000); J. M. Ugalde, I. B. Alkorta, and J. Elguero, Angew. Chem., Int. Ed. **39**, 717 (2000); J. Poater, X. Fradera, M. Solá, M. Duran, and S. Simon, ChemPhysChem **369**, 248 (2003); L. F. Pacios, O. Gálvez, and P. C. Gómez, J. Chem. Phys. **122**, 214307 (2005); R. Parthasarathi, V. Subramanian, and N. Sathyamurthy, J. Phys. Chem. A **110**, 3351 (2006); S. J. Grabowski, W. A. Sokalski, E. Dyguda, and J. Leszcynski, J. Phys. Chem. B **110**, 6444 (2006); S. J. Grabowski, W. A. Sokalski, and J. Leszcynski, J. Phys. Chem. A **110**, 4772 (2006); J. Chen, I. Ratera, J. Y. Park, and M. Salmeron, Phys. Rev. Lett. **96**, 236102 (2006).

[48] P. Gilli, V. Bertolasi, V. Ferretti, and G. Gilli, J. Am. Chem. Soc. **116**, 909 (1994); C. L. Perrin and J. B. Nielson, Annu. Rev. Phys. Chem. **48**, 44 (1997); P. A. Frey, Magn. Reson. Chem. **39**, S190 (2001); T. Steiner, Angew. Chem., Int. Ed. **41**, 48 (2002); B. Schiott, B. B. Iversen, G. K. H. Madsen, F. K. Larsen, and T. C. Bruice, Proc. Natl. Acad. Sci. U.S.A. **95**, 12799 (1998); G. K. H. Madsen, G. J. McIntyre, B. Schiott, and F. K. Larsen, Chem.-Eur. J. **13**, 5539 (2007).

[49] R. P. Muller and A. Warshel, J. Phys. Chem. **99**, 17516 (1995); J.-K. Hwang, G. King, S. Creighton, and A. Warshel, J. Am. Chem. Soc. **110**, 5297 (1988).

[50] J. M. García-Lastra, T. Wesolowski, M. T. Barriuso, J. A. Aramburu, and M. Moreno, J. Phys.: Condens. Matter **18**, 1519 (2006).

[51] O. Vendrell, F. Gatti, D. Lauvergnat, and H.-D. Meyer, J. Chem. Phys. **127**, 184302 (2007); O. Vendrell, F. Gatti, and H.-D. Meyer, *ibid.* **127**, 184303 (2007); Angew. Chem., Int. Ed. **46**, 6918 (2007).